GU J Sci, Part C, 10(2): 216-229 (2022)

Gazi University

Journal of Science

PART C: DESIGN AND TECHNOLOGY

http://dergipark.gov.tr/gujsc

An EBSD Study on Crystallization of CaO-MgO-Al_2O_3-SiO_2 (CMAS) Glass

Sinem BAŞKUT[1,*], Emrah DÖLEKÇEKİÇ[1], Göktuğ GÜNKAYA[2], Taner KAVAS[3]

[1]*Eskisehir Technical University, Faculty of Engineering, Department of Materials Science and Engineering, 26555, ESKİSEHİR*

[2]*Anadolu University, Faculty of Fine Arts, Department of Glass, 26470, ESKİSEHİR*

[3]*Afyon Kocatepe University, Faculty of Engineering, Department of Materials Science and Engineering, 03200, AFYONKARAHİSAR*

Article Info

Research article
Received:22/03/2022
Revision:14/04/2022
Accepted:20/06/2022

Keywords

Anorthite
EBSD
Surface crystallization
Glass-ceramics
DTA

Abstract

This study applied heat treatment to the CMAS parent glass produced using brucite with calcite, kaolin, ulexite natural raw materials, and commercial MgF_2, considering the DTA measurements. The crystallization behaviour and the growth directions of the crystals were investigated. XRD analyses and SEM investigations revealed that the anorthite crystals were formed during heat treatment, and glass-ceramic was obtained in the CAS system by surface crystallization. According to EBSD measurements, the {100} faces of the some anorthite crystals just below the surface have a relatively higher ratio of lying parallel to the surface than their edges ({110}) and corners ({111}). These crystals grew by orienting in the same direction to the inner region of the remaining glass. However, many crystals exhibited random orientation. The tendency of crystals' same planes to lie parallel to the surface was slightly less in the inner regions than those on the surface.

1. INTRODUCTION

Glass-ceramics are inorganic, polycrystalline materials obtained by the controlled crystallization of glasses, including the homogeneous or heterogeneous nucleation and crystal growth stages [1]. One of the main crystallization methods used in production of glass-ceramics is bulk crystallization, which takes place within the entire glass structure with the contribution of the nucleating agent. Another is surface crystallization, which is only generated at and/or near the glass surface without the nucleating agent [2-4]. They generally exhibit superior mechanical, thermal, optical properties and chemical stability compared to parent glass with the contribution of crystallization [2]. Due to these properties, glass-ceramics have become highly preferred materials in many technological areas such as electronic, biomedical, photonics, optic and aerospace industries, and their commercial used applications such as cookware and architectural components [5-8].

Different glass-ceramic systems can be obtained by using natural raw materials in the initial composition of the parent glass. The amounts of these raw materials are tailored depending on their chemical content to form the proportions of the candidate phases that will form the parent glass [9-14]. During preparing the glass-ceramics, the heat treatment applied to the parent glass can be considered in terms of nucleation and crystal growth temperatures or the type of used nucleating agent can determine the crystallization behavior of the parent glass' initial composition [11, 12]. In a study [13], where CaO-MgO-Al_2O_3-SiO_2 (CMAS) glass was produced by using quartz, feldspar, calcite, dolomite natural minerals and industrial slag as starting raw materials and CaF_2, ZrO_2, P_2O_5 as nucleation agents, CMAS glass-ceramics were obtained by bulk crystallization with the help of heat treatment.

Besides all these, in recent years, since the orientation of the formed crystals is a decisive parameter for some properties of glass-ceramics, whether the crystals are oriented while growing has become a

*Corresponding author, e-mail: skayhan@eskisehir.edu.tr
DOI:10.29109/gujsc.1091233

considerable research topic [15-17]. Especially in non-ferroelectric glass-ceramics, crystal orientation can lead to forming a piezoelectric and/or pyroelectric surface layer [15, 17, 18]. Surface crystallization is a highly preferred method of obtaining glass-ceramics where the growth orientation of crystals is essential [15-17]. During surface crystallization, crystals grow into the inner region of the parent glass after nucleation occurs on or near the surface [19]. Although the crystallographic information of the formed crystals in glass-ceramics can be accessed traditionally with x-ray diffraction (XRD) technique, the fact that the results in the XRD technique depend on the quantity of crystals limits its use [20]. On the other hand, the electron backscatter diffraction (EBSD) technique, a scanning electron microscope-based tool, is the most powerful technique used to determine the nucleation or growth direction of crystals formed near or on the glass surface [21-23]. EBSD can collect diffraction information from particles smaller than 1 μm, regardless of quantity and present the plane and orientation information of glass-ceramic crystals with high precision [20]. However, the surface sensitivity of glass-ceramics to the high electron energy used in EBSD analyzes can cause pattern degradation, which requires great attention in the selected EBSD analysis parameters [16]. Considering this information, one of the motivations of this study was to obtain a glass-ceramic system by the heat treatment applied to CMAS parent glass produced by using natural raw materials brucite with calcite, kaolin, ulexite and commercial MgF_2 without nucleation agent. Another focus in this study was to determine the phase and orientation information of the crystals formed in the structure of the glass-ceramic using the EBSD technique. For these purposes, based on the nucleation and crystallization temperatures determined by differential thermal analysis (DTA) analysis, the parent glass was gradually heat-treated, and the realized crystallization mechanism was revealed by XRD and scanning electron microscope (SEM) examinations. EBSD analyses were performed on glass-ceramic surfaces made as smooth as possible in two different mechanical polishing times.

2. MATERIALS AND METHODS

In the first stage of the study, it was first planned to create a composition based on the oxide and compounds ratios (Table 1) determined by Stebbins et al. [23], to obtain a glass in the CMAS system. For this purpose, brucite with calcite, kaolin (CC 31) and ulexite, whose x-ray fluorescence (XRF) results were listed in Table 2 and also MgF_2 were used as starting raw materials and parent glass batch calculations were made according to the desired amounts of oxide and compounds presented in Table 1. A total of 130 g parent glass composition was prepared to consist of 30 g brucite with calcite, 60 g kaolin, 30 g ulexite and 10 g MgF_2. The starting powders were mixed and melted in a platinum crucible at 1450 ºC for 2 h in an air atmosphere (Protherm, atmosphere controlled vertical glass melting furnace). A frit glass was obtained by pouring the viscous liquid into the cool water.

The heat treatment conditions applied to the parent glass were determined based on the DTA (Netzsch, STA 409PG) analysis. XRD measurements were carried out to the ground powdered form (Rigaku, RINT-2000) and surface (Bruker, axs) of the heat-treated glass between 10-60 degrees (2Θ) under the conditions of 40 kV accelerating voltage, 30 mA current, 1°/min scan speed and 0.02 step size.

While the morphological images of the surface and fractured surface of the heat-treated sample were obtained by using a secondary electron detector (SE-SEM), the cross section which was polished with various polishing steps from coarse to the fine in the automatic polisher was examined by backscatter electron image (BSE-SEM) in the SEM (Zeiss, SUPRA 50 VP). Energy dispersive x-ray spectroscopy (EDS-SEM, Oxford Instruments, INCA ENERGY) analyses were performed to different regions on the polished cross section of glass-ceramic. EBSD (Oxford Instruments, INCA HKL NordlysS attached to the SEM) analyses of the heat-treated glass surface were conducted at variable pressure mode without coating on sample that was polished at two different times. In the first EBSD analysis, 1 μm diamond polishing solution followed by a colloidal silica step was performed for 15 min in a controlled manner to avoid the anorthite crystals remove from the sample surface. After the first EBSD investigation, the polishing time applied to the same sample was extended to 30 min and the second EBSD analysis was carried out. The areas covered by the crystals in the images showing the regions where EBSD analyzes were performed were determined with the ImageJ program.

Table 1. *Oxides and compounds that form the desired parent glass composition and their quantities [24].*

Oxides	***Parent glass Composition (wt %)***
SiO_2	*32.40*
Al_2O_3	*22.75*
Fe_2O_3	*0.61*
CaO	*15.29*
MgO	*7.55*
Na_2O	*0.98*
K_2O	*0.30*
TiO_2	*0.30*
MnO	*0.003*
P_2O_5	*0.003*
SO_3	*0.017*
Cr_2O_3	*0.039*
B_2O_3	*10.22*
SO_4	*0.069*
SrO	*0.276*
MgF_2	*9.21*
Total	***100.00***

Table 2. *XRF results of the raw materials used during the study.*

Oxides	***Brucite with Calcite***	***Kaolin (CC 31)***	***Ulexite***
SiO_2	*0.3*	*47. 5*	*4.0*
Al_2O_3	*0.13*	*36.3*	*0.25*
Fe_2O_3	*0.009*	*1.24*	*0.04*
CaO	*36*	*0.156*	*19*
MgO	*24.5*	*0.138*	*2.5*
Na_2O	*0.05*	*-*	*3.5*
K_2O	*0.01*	*3.14*	*-*
TiO_2	*0.01*	*0.317*	*-*
Cr_2O_3	*-*	*0.042*	*-*
B_2O_3	*-*	*-*	*37*
Ignition loss	*38.99*	*11.167*	*33.71*
Total	***100***	***100***	***100***

3. RESULTS

The DTA analysis graph showing the temperature dependent behavior of the parent glass is given in Figure 1. DTA analysis revealed that nucleation and crystallization occurred as exothermic reactions at around 750 and 900 ºC, respectively. When the temperature is increased from 900 ºC (where crystallization takes place) to 1035 ºC, the sudden change towards the endothermic reaction can be explained by the melting of the glass at this temperature. Additionally, the exothermic event observed at ~1050 ºC indicated that the second crystallization of the glass occurred at this temperature. Considering the DTA analysis results, the heat treatment conditions applied to the parent glass are presented in Table 3. The heat-treatment process was

carried out in three steps. Firstly, the temperature was increased to glass transition temperature (650 ºC) in 120 min and waited at this temperature for 1 h to promote nucleation. Then, the temperature was increased to 750 ºC in 20 min and waited for 1 h. In the third step, the temperature was increased to 900 ºC in 20 min and waited at this temperature for 2 h. Lastly, the sample was taken out after cooling to room temperature for 2 h in the furnace environment.

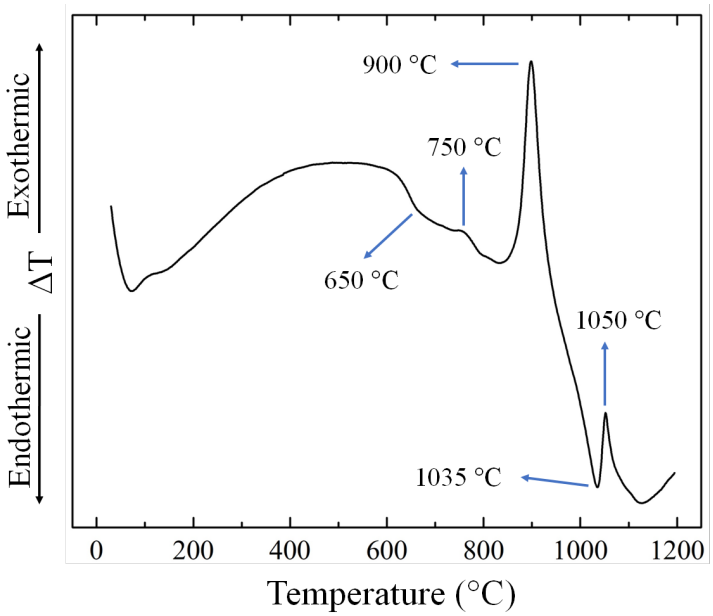

Figure 1. *DTA graph showing temperature dependent behavior of the CMAS parent glass.*

Table 3. *Heat treatment conditions applied to CMAS parent glass*

Heat Treatment	***Temperature (°C)***	***Duration Time (h)***
T_g	*650*	*1*
Nucleation	*750*	*1*
Crystal Growth	*900*	*2*

In order to determine the possible crystallization, the heat-treated glass was first ground and XRD analysis was performed to this powder form. However, the XRD pattern of the powder form (Fig. 2 a) indicated the existence of purely amorphous structure. On the other hand, since some color changes were observed on the surface of the heat-treated glass, it was concluded that the possible crystallization was below the detection limit of XRD. Therefore, XRD analysis (Fig. 2 b) was performed directly to the surface of the heat-treated glass and the presence of anorthite phase revealed that a glass-ceramic was obtained in the CAS system. XRD outputs indicated that surface crystallization may have occurred during heat treatment. The round shape of the glass-ceramic surface resulted in a noisy XRD pattern. It has been noticed that there was no driving force for the formation of a glass-ceramic in the MAS or CMAS systems under the composition ratios and heat treatment conditions applied during the study.

The morphological SE-SEM images at low (Fig. 3 a) and high (Fig. 3 b) magnifications taken from the surface of anorthite glass-ceramic showed that anorthite crystals formed on the surface of the parent glass in two different geometries as circular and elongated. Further, it was noticed that the existence of protrusions on the circular anorthites (Fig. 3 a, b). Figures 3 c and d present the SE-SEM and BSE-SEM images taken from the fractured and polished cross-sections of glass-ceramic, respectively. The cross-section images confirmed that glass-ceramic was obtained by surface crystallization. In addition, it was

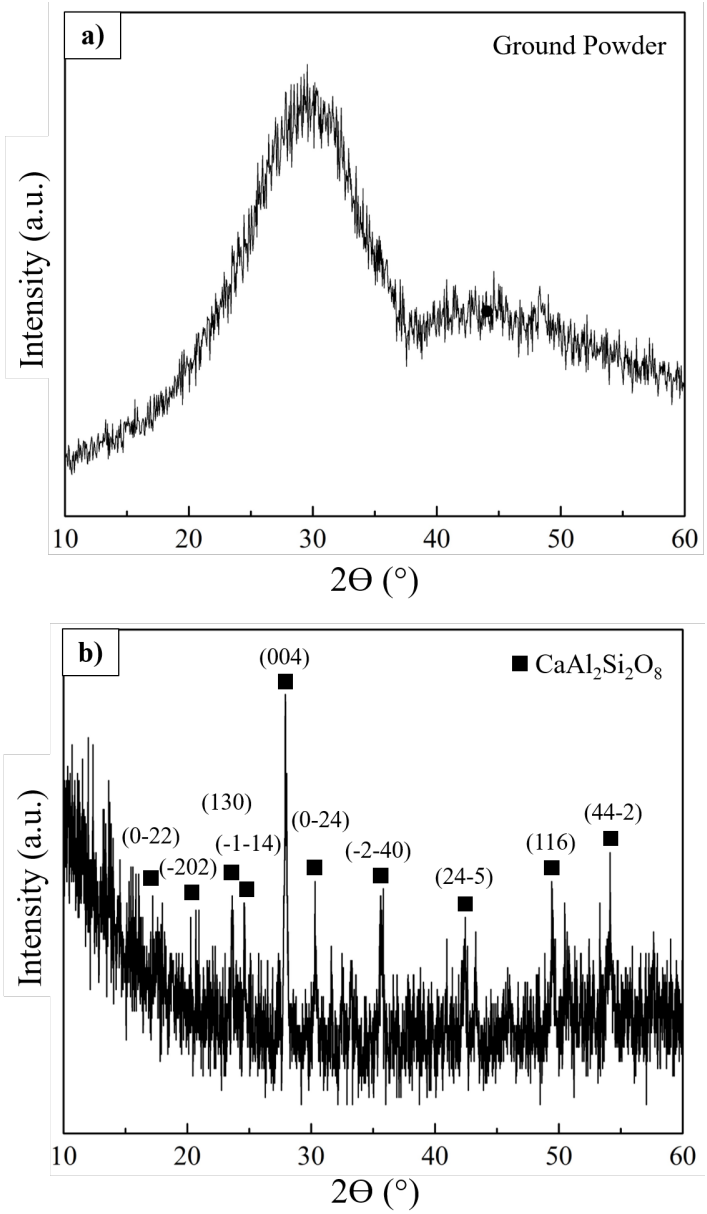

Figure 2. *XRD pattern obtained from (a) ground powder form and (b) surface of heat-treated glass.*

determined that the anorthite crystals formed on and near the surface grow to about 50-100 µm towards the bulk, and they extend to a depth of more than 150 µm in some regions. When the morphological images of the surface and the BSE image of the cross-section were evaluated together, it was determined that the anorthite crystals formed as non-homogeneous dispersed clusters on and near the surface of glass-ceramic and there was a significant amount of remaining glass between them. Figure 3 e and f show the results of the qualitative and quantitative EDS-SEM analyses performed on the remaining glass in the region where the anorthite crystals are dispersed and in the bulk. The analyzed regions were indicated by numbers 1 and 2 in the BSE image of the cross section given in Figure 3 d. At least three measurements were performed to each region and the averages of the obtained quantitative values were used during the study. The EDS-SEM results revealed that the chemical composition of the remaining glass exhibits differences in regions 1 and 2. The peak intensities (Fig. 3 e) and quantitative results (Fig. 3 f) of elements Ca, Al, Si and O in region 1, where nucleation occurred and anorthite crystals are grown, have been found lower than in region 2, which was less affected by crystallization. This showed that a certain amount of these elements in the near-surface region were consumed in the formation of anorthite crystals and that the chemical compositions of the inner regions of the glass-ceramic are closer to those of the parent glass. On the other

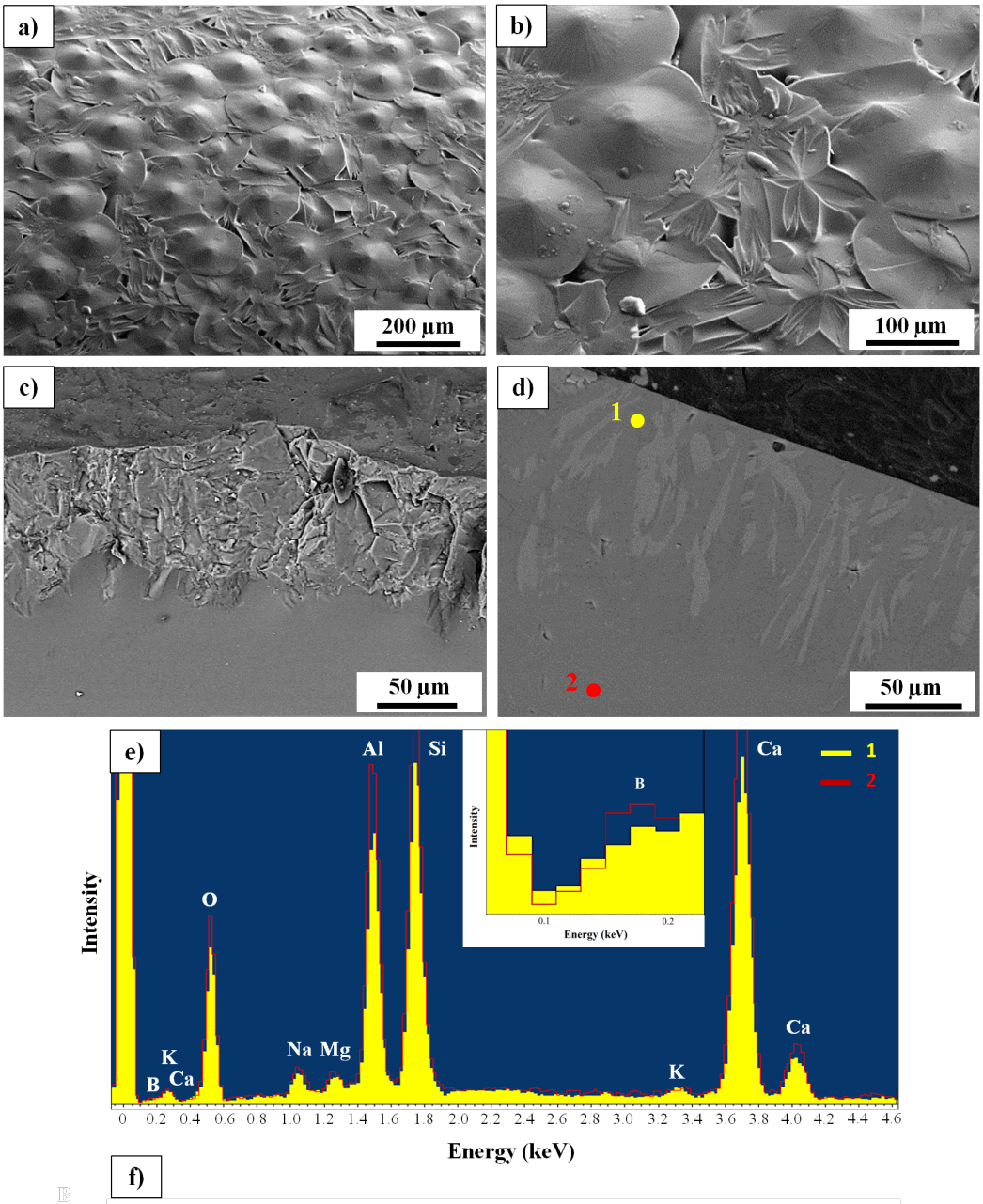

f)

Regions	Elements (wt.%)							
	Al	Si	Ca	O	Mg	Na	K	B
1	11.2±0.6	13.1±0.5	22.3±0.4	45.4±1.3	2.2±0.2	3.1±0.4	2.4±0.3	0.3±0.03
2	11.7±0.3	13.5±0.3	22.8±0.2	45.9±1.5	1.3±0.3	2.1±0.2	2.0±0.1	0.7±0.05

Figure 3. *(a) Low and (b) high magnification SE-SEM images obtained from the surface of the heat-treated glass. (c) SE-SEM and (d) BSE-SEM images taken from fractured and cut-polished cross sections of heat-treated glass, respectively. (e) EDS-SEM compared spectra and (f) quantitative results of the region 1 and 2 indicated in Figure 3 d.*

hand, the fact that the peak intensity of element boron (B) in the compared spectra was slightly higher in region 2 than in region 1 (enlarged compared spectra in Fig. 3 e) indicated that the B in the initial composition may be one of the parameters affecting the crystallization behavior of the parent glass. It is known that a certain amount of B content has the function of suppressing the crystallization by increasing

the durability of glass [25-27]. Due to the release of B during the heat treatment, the decrease in its content at and near the surface of the glass may have allowed anorthite crystals to form in these regions with an exact shape. The increase in the amount of B towards the inner regions of the remaining glass may have led to a decrease in crystallization and an increase in the amount of remaining glass. Since the lowest detection limit of the EDS detector used in the study was atomic number 5 (B), interpretation was made by considering the peak intensity differences between two regions instead of the quantitative results of element B.

The positioning of the anorthite crystals on the glass-ceramic surface has led to the need to investigate whether it grows in the remaining glass by orientation from the surface to the deep regions. To observe in detail EBSD analyses were performed on the surface of glass-ceramics. For EBSD analysis, the requirement that the surface of the sample should be smooth and at the same time to prevent the anorthite crystals being swept from the surface during mechanical polishing led to the application of a short polishing time of 15 min. The EBSD analysis results of this sample were given in Figure 4. The SE-SEM image (Fig. 4 a) showed that the protrusions on the surface of the anorthite crystals were still vaguely present. The microstructure details, which are not visible in the SE-SEM image and were highlighted by yellow arrows (Fig 4 b), have been successfully revealed with the pattern quality map, since EBSD operates at high angles and very small interaction volume [23, 28, 29]. The fact that all crystals were resolved in the pattern quality map indicated that no second phase was formed in addition to anorthite during the heat treatment, supporting the XRD result. However, the EBSD technique is negatively affected by microstructure imperfections, sample preparation inadequacies, and surface topography. Even though the sample is polished, some anorthite crystals visible in the SE-SEM image could not be fully resolved (shown with green arrows in Fig. 4 b) in the pattern quality map as a result of the existence of height differences between some regions in the microstructure and remaining protrusions on the anorthite surfaces. In addition, while the SE-SEM images taken from the non-polished surface (Fig. 3) of the glass-ceramic showed that almost the entire surface is covered with anorthite phase, the SE-SEM image and diffraction pattern quality map (Fig. 4 a, b) indicated that some remaining glass phases become visible between the anorthite crystals with the removal of a few micrometers from the surface by mechanical polishing. Figures 4 c and d show the phase map and the quantities of phases (%) that exist in the examined region, respectively. In the phase map, the anorthite phase was represented by a yellow color, while the black color was used for the amorphous remaining glassy phase+the unresolved crystals. 68 % of the examined area was composed of anorthite crystals and 32 % contains glassy phase+unresolved crystals indicated with green arrows in the pattern quality map (Fig. 4 b). The area covered by the anorthite crystals on the same image (Fig. 4 a) was determined as ~ 74 % using ImageJ software, supported the EBSD analysis results.

The directions in which the crystal orientation maps were obtained are schematically represented in Figure 4 e. Further, the positions of the planes of the anorthite crystals according to the examined directions as normal, rolling and transverse are determined by the color key given in Figure 4 f. Each measured direction in the crystalline orientation map is associated with the red, green, blue colors and the soft color gradations between them found in the color key. Figure 4 g, i, k and h, j, l showed the crystal orientation maps and related inverse pole figures in the normal (Fig. 4g, h), rolling (Fig. 4 i, j) and transverse (Fig. 4 k, l) directions, respectively. When firstly considering the normal direction crystal orientation map, it has been observed that anorthite crystals have green, red, blue and tones of these colors. Nevertheless, the slight predominance of the green color tones in the normal crystal orientation map (Fig. 4 g) and a slight polarity in the regions of inverse pole figure (Fig. 4 h) corresponding to the region expressed by green color and its tones in the color key (Fig. 4 f) indicated that the face of the anorthite crystal {100} has a relatively higher ratio of lying parallel to the surface than the edges ({110}) and corners ({111}) of the crystal. On the other hand, it was observed that anorthite crystals indicated with white arrows and encoded with green color in the normal direction crystal orientation map have a green and pinkish red tone as little dominance in the rolling and transverse direction crystal orientation maps (Fig. 4 i, k), respectively. These findings firstly proved that the planes of these anorthite crystals expressing the same edges and corners and whose {100} faces are parallel to the surface, were grown to the inner region of the remaining glass by orienting in a

similar direction. In addition, some grains represented with red color (shown with yellow arrows in Fig. 4 g) in the normal direction crystal orientation map was coded with only blue and green colors in the rolling (Fig. 4 i) and transverse (Fig. 4 k) directions crystal orientation maps. This pointed out that similar faces of these anorthite crystals were formed by orientation in the same direction. Moreover, according to color differences in the three orientation maps, different planes of anorthite crystals were oriented parallel to the surface. This showed that different planes of many anorthite crystals coded with different colors were formed on the surface and extended towards to deep regions of the remaining glass by random orientation during the heat treatment.

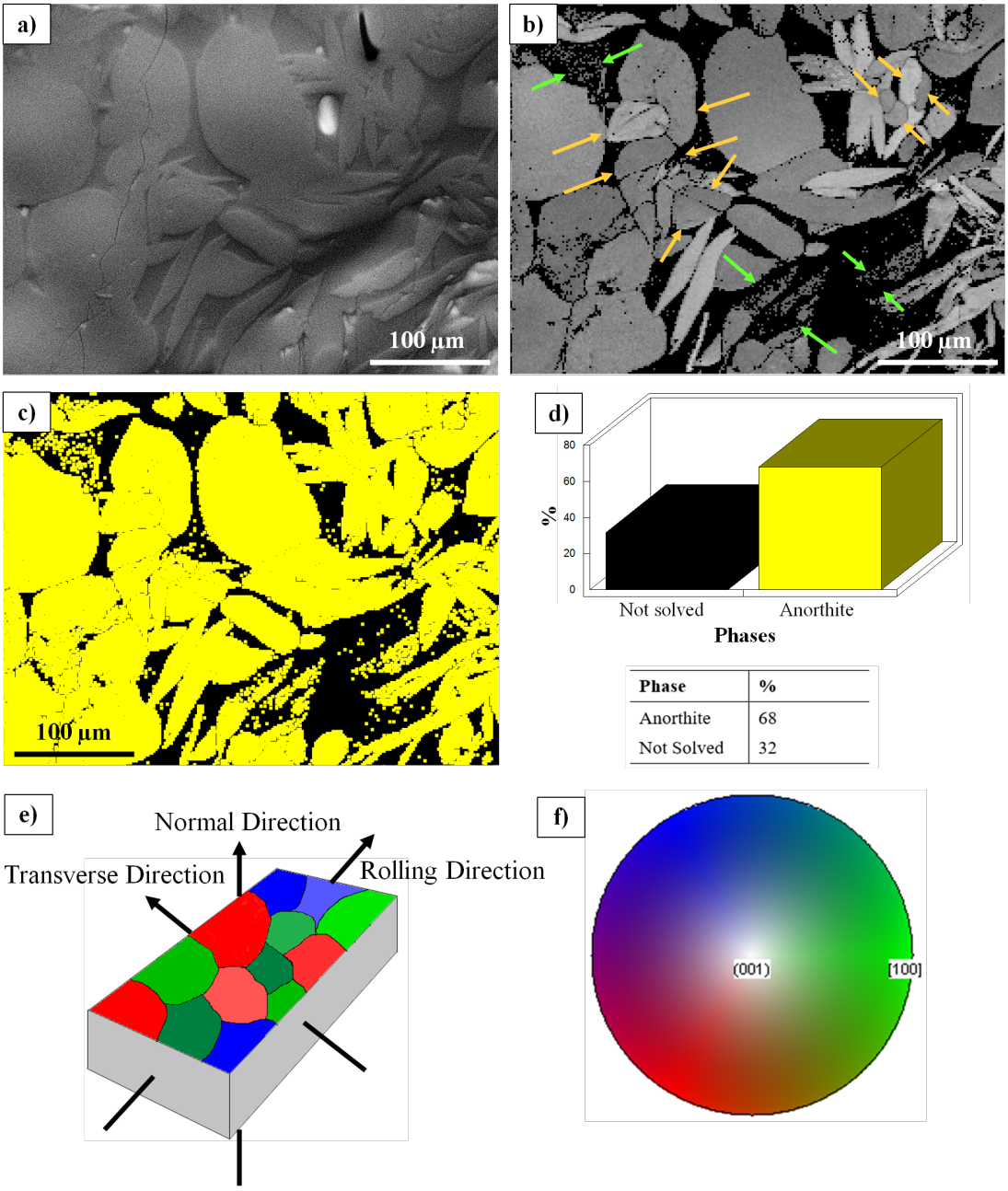

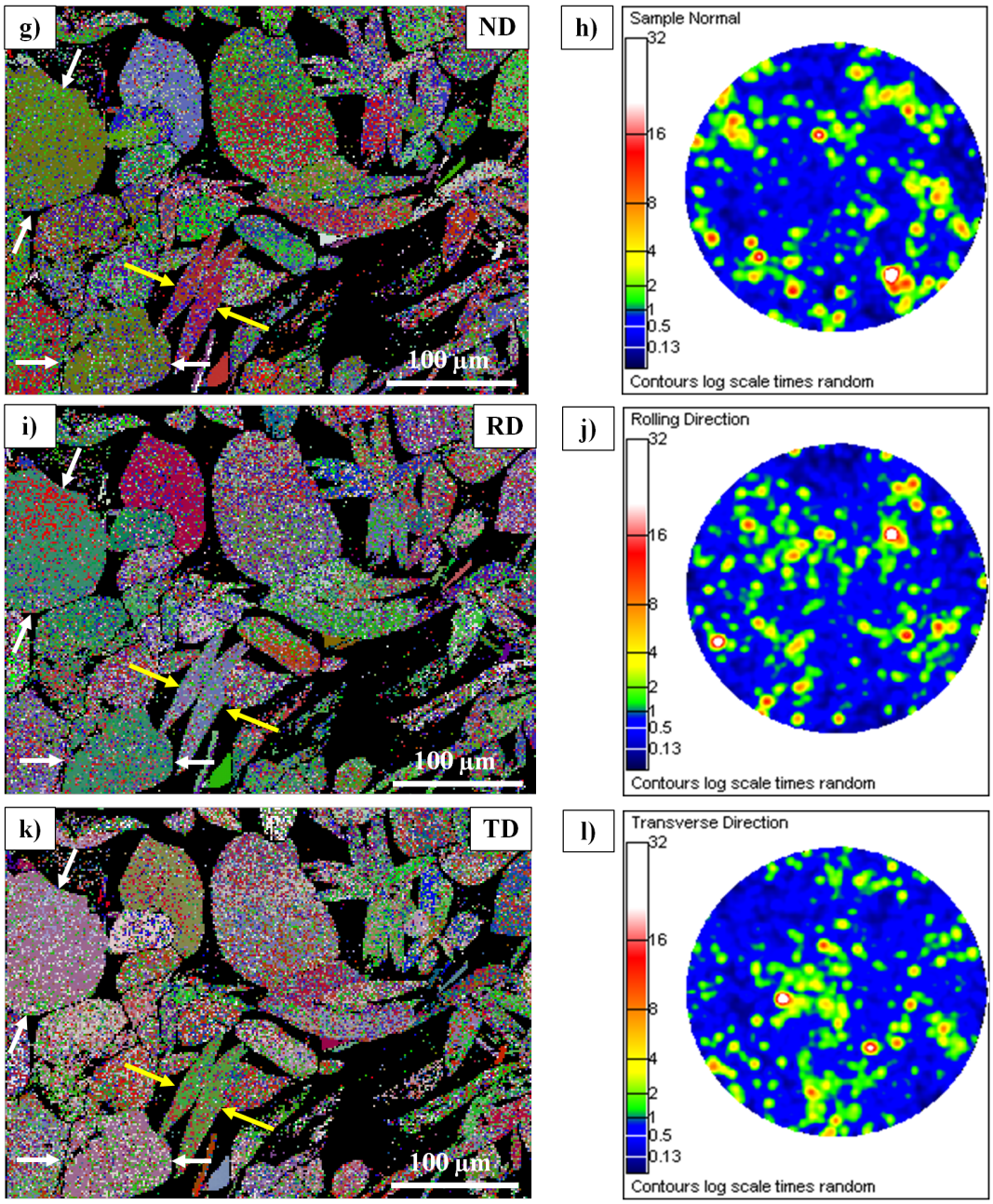

Figure 4. *(a) Electron image (b) pattern quality map and (c) phase map obtained from the examined region. (d) Quantities of phases (%) exist in the examined region. (e) Measurement directions of EBSD technique (f). Color key for crystal orientation maps. (g, i, k) Crystal orientation maps and (h, j, l) inverse pole figures in the (g, h) normal, (i, j) rolling and (k, l) transverse directions, respectively.*

To investigate the distribution of the anorthite crystals further below the surface, the polishing time of the glass-ceramic surface was increased to 30 min (Fig. 5). According to SE-SEM image and EBSD pattern quality map of the examined region (Fig. 5 a, b), only elongated anorthite crystals remained on the glass-ceramic surface with the extension of the polishing time. Considering this information, it can be deduced that first elongated anorthite crystals were formed on and near the surface during heat treatment, and in the following process, these crystals only found the opportunity to grow on the outer surface and could be transformed into a circular shape. This and the increment in the amount of remaining glass phase surrounding the anorthite crystals when going to the deep region with the increase of the polishing time supported the interpretation made about the effect of element B on crystallization. In addition, the elongated

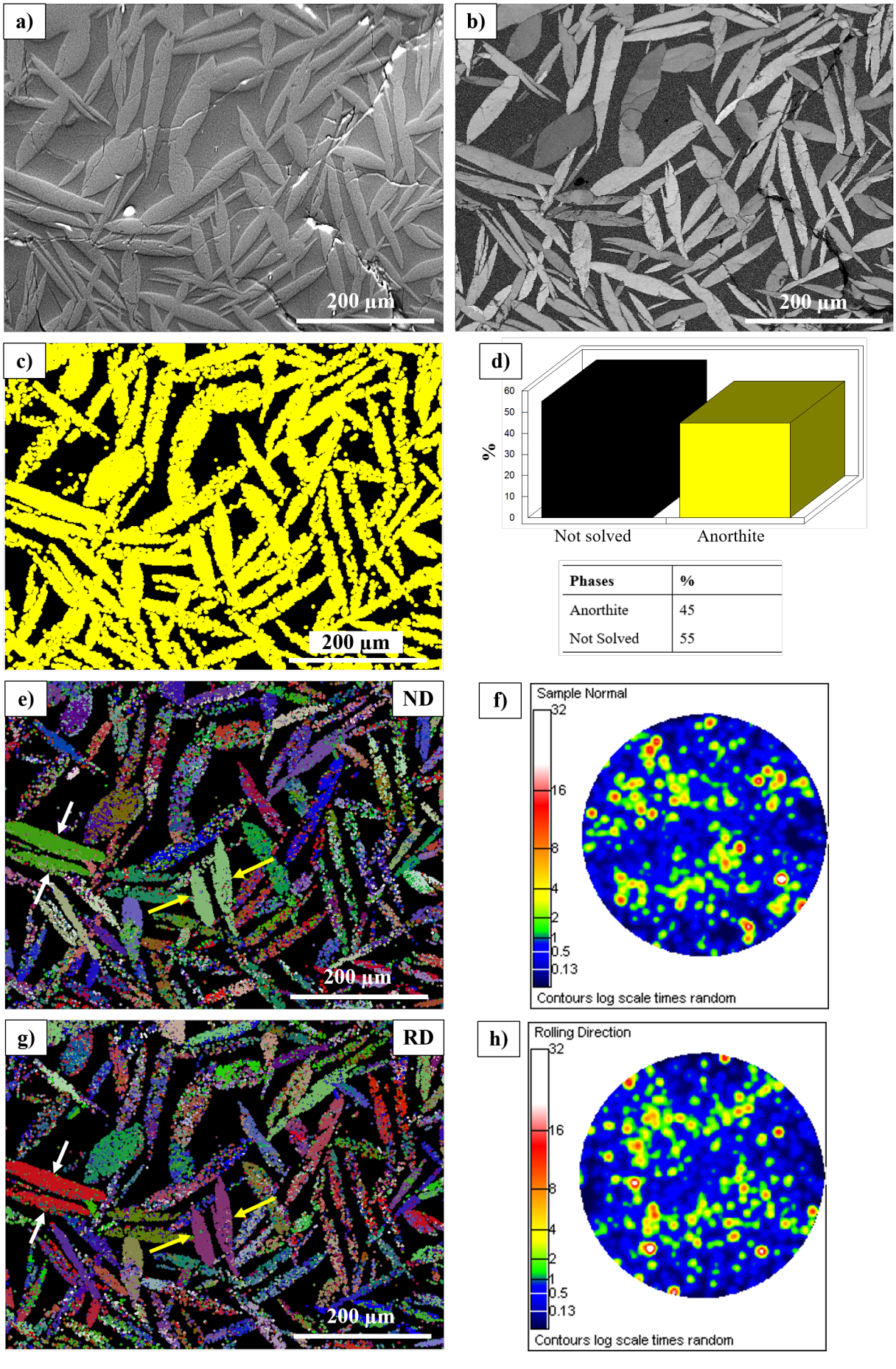

Phases	%
Anorthite	45
Not Solved	55

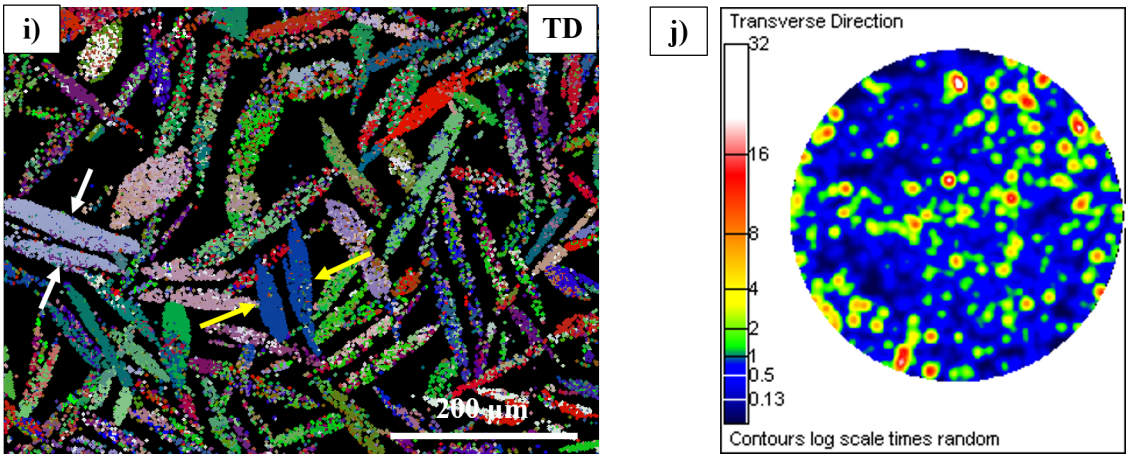

Figure 5. *(a) Electron image (b) pattern quality map and (c) phase map obtained from the examined region. (d) Quantities of phases (%) exist in the examined region. (e, g, i) crystal orientation maps and (f, h, j) inverse pole figures in the (e, f) normal, (g, h) rolling and (i, j) transverse directions, respectively.*

crystals on the outer surface may not have transformed to a circular shape because of insufficient space. The elongated anorthite crystals seen in Fig. 5 could be a continuation of the circular crystals shown in Figure 4 or different anorthite crystals formed below the surface. Pattern quality map (Fig. 5 b) revealed that anorthite crystals could be resolved because of removing some of the factors that negatively affect the EBSD analysis performed on the sample surface with the increase in polishing time. In the first EBSD analysis (Fig. 4 c and d) although the unresolved anorthite crystals were also included in the amount of black region formed by the amorphous glass, the obtained percentage (32 %) was lower than the amount of anorthite. In the second EBSD analysis results, since all anorthite crystals can be resolved, the black color not solved regions in the phase map belongs only to the glassy phase due to its amorphous nature (Fig. 5 c). Nevertheless, the amount of glassy phase in the studied region was measured as 55 %, and it was more than the anorthite phase (Fig. 5 d). ImageJ measurements performed in the same region showed that the areas covered by the anorthite crystals, and the glassy phase were approximately 47 and 53 %, respectively, consistent with the EBSD analysis results. With the extension of the polishing time by 15 min, the amount of glassy phase between the anorthite crystals increased by approximately 72 %, although only a few micrometer materials were removed from the surface. The normal, rolling and transverse direction orientation maps (Fig. 5 e, g, i) obtained in this EBSD analysis showed that some anorthite crystals grew by orientation, supporting the results of the first analysis. For example, two anorthite crystals shown with white arrows in the orientation maps were colored with green in the normal direction crystal orientation map (Fig. 5 e), with red in the rolling direction crystal orientation map (Fig 5 g) and with light purple in the transverse direction crystal orientation map (Fig. 5 i). Likewise, two anorthite crystals shown with yellow arrows in the three crystal orientation maps were represented with the same color in all crystal orientation maps. The concentration regions in the inverse pole figures also supported this orientation behavior (Fig. 5 f, h, j). This showed that these anorthite crystals, indicated by arrows have formed and grown as their {100} faces, {110} edges and {111} corners parallel to each other and oriented in the same direction. However, compared to the surface polished for 15 min slightly higher color differences in the normal direction orientation maps, showed that the different planes of the crystals formed below the surface also lie parallel to the surface. Although the RD and TD orientation maps showed that some of these crystals were oriented in such a way that their same planes were parallel to each other, it has been observed that the tendency of lying the same planes parallel to the surface decreases as moved deeper region from the surface. The sparseness of the anorthite crystals from the surface to deeper regions and the increase in the amount of remaining glass can be assumed as the reason for the random orientation in inner regions. This result was consistent with the work [17] in which EBSD investigated the growth directions of fresnoite crystals in a

$2BaO_3$ TiO_2 $2.75SiO_2$ glass. In that study, the orientation degrees of the fresnoite crystals decreased in the deep regions.

4. CONCLUSIONS

In this study, brucite with calcite, kaolin, ulexite natural raw materials and commercial MgF_2 were mixed in certain proportions considering the desired glass composition and parent glass was obtained in the CMAS system. Firstly, the nucleation and crystallization temperatures were determined by performing DTA measurement to the parent glass and heat treatment was applied according to the DTA results. XRD and SEM investigations revealed that anorthite crystals were formed during heat treatment and glass-ceramic was obtained in the CAS system with the realization of surface crystallization.

The crystal orientation maps obtained in EBSD analyses showed that some anorthite crystals formed on the surface with their same planes parallel to each other and grew to deeper regions of the remaining glass by being oriented in the same direction. However, the variety of colors in the normal, rolling and transverse directions and the polarization states in the related inverse pole figures revealed that most of them were formed by the orientation of the same planes in different directions. EBSD analysis belongs to the inner regions of glass-ceramic showed that the possibility of the same planes of the crystals to lie parallel to the surface decreased as being far from the surface.

REFERENCES

[1] Deubener, J., Allix, M., Davis, M.J., Duran, A., Höche, T., Honma, T., Komatsu, T., Krüger, S., Mitra, I., Müller, R., Nakane, S., Pascual, M.J., Schmelzer, J.W.P., Zanotto, E.D., Zhou, S. (2018). Updated definition of glass-ceramics. Journal of Non-Crystalline Solids, 501, 3–10. https://doi.org/10.1016/j.jnoncrysol.2018.01.033.

[2] Sakamoto, A., Yamamoto, S. (2010). Glass–Ceramics: Engineering Principles and Applications. International Journal of Applied Glass Science, 1(3), 237–247. https://doi.org/10.1111/j.2041-1294.2010.00027.x.

[3] Mcmillan, P.W. (1982). The Crystallisation of Glasses. Journal of Non-Crystalline Solids, 52, 67-76. https://doi.org/10.1016/0022-3093(82)90281-2.

[4] Zanotto, E.D. (2000). Experimental studies of surface nucleation and crystallization of glasses. in Nucleation and Crystallization in Glass and Liquids. Journal of American Ceramic Society, 65-74. ISBN-13: 978-0944904572.

[5] Davis, M.J., Zanotto, E.D. (2017). Glass-ceramics and realization of the unobtainable: Property combinations that push the envelope. Materials Research Society, 42, 195-199. https://doi.org/10.1557/mrs.2017.27.

[6] Fernandes, M.H.V., Silva, A.M.B. (2016). Glass-Ceramics: Concepts and Practical Aspects. in Overall Aspects of Non-Traditional Glasses: Synthesis, Properties and Applications. Bentham e-books, 39-65. ISBN: 978-1-68108-208-0.

[7] Ozabaci, M., Aksan, M.A., Kirat, G., Kizilaslan, O., Yakinci, M.E. (2006). Preparation and characterization of CaO-Al_2O_3-SiO_2 (CAS) glass-ceramics. Journal of Non-Crystalline Solids, 454, 8–12. https://doi.org/10.1016/j.jnoncrysol.2016.10.019.

[8] Morsi, M.M., Khater, G.A., Range, K.J. (2001). Glass ceramics in the system diopside, anorthite-orthoclase prepared by using some industrial waste materials. Glass Technology, 42(6), 160-164.

[9] Pinckney, L.R. (2001). Glass Ceramics, Encyclopedia of Materials: Science and Technology. Elsevier, 3535-3540. https://doi.org/10.1016/B0-08-043152-6/00629-X.

[10] Marghussian, V. (2015). Nanoglass Ceramics Processing Properties and Applications. Elsevier, 2-61.

[11] Leonelli, C., Manfredini, T., Paganelli, M., Pozzi, P., Pellacani, G.C. (1991). Crystallization of some anorthite-diopside glass precursors. Journal of Materials Science, 26, 5041-5046.

[12] Carter, C.B., Norton, M.G. (2013). Processing Glass and Glass-Ceramics in Ceramic Materials Science and Engineering. Springer, New York, 389-409. https://doi.org/10.1007/978-0-387-46271-4_26

[13] Xiao, H., Cheng, Y., Yang, Q., Senda, T. (2006). Mechanical and tribological properties of calcia–magnesia–alumina–silica-based glass–ceramics prepared by in situ crystallization. Materials Science and Engineering:A, 423(1–2),170-174. https://doi.org/10.1016/j.msea.2005.09.131.

[14] Merkit, Z.Y., Toplan, H.O., Toplan, N. (2018). The crystallization kinetics of $CaO–Al_2O_3–SiO_2$ (CAS) glass–ceramics system produced from pumice and marble dust. Journal of Thermal Analysis and Calorimetry, 134, 807–811. https://hdl.handle.net/20.500.12619/69704.

[15] Russel, C., Wisniewski, W. (2021). How Can Surface-Crystallized Glass-Ceramics Be Piezoelectric?. Crystal Growth Design, 21, 2405−2415. https://doi.org/10.1021/acs.cgd.1c00029.

[16] Wisniewski, W., Russel, C. (2015). EBSD measurements of phlogopite glass ceramics. The Royal Society of Chemistry, 17, 8671–8675. https://doi.org/10.1039/c5ce01763g.

[17] Wisniewski, W., Nagel, M., Volksch, G., Russel, C. (2010). Electron Backscatter Diffraction of Fresnoite Crystals Grown from the Surface of a $2BaO_3$ TiO_2 $2.75SiO_2$ Glass. Crystal Growth Design, 10(3), 1414-1418. https://doi.org/10.1021/cg901407d.

[18] Russel, C. (1997). Oriented crystallization of glass. A review. Journal of Non-Crystalline Solids, 219, 212-218. https://doi.org/10.1016/S0022-3093(97)00271-8.

[19] Muller, R., Zanotto, E.D., Fokin, V.M. (2000). Surface crystallization of silicate glasses: nucleation sites and kinetics. Journal of Non-Crystalline Solids, 274, 208−231. https://doi.org/10.1016/S0022-3093(00)00214-3.

[20] Peruzzo, L., Fenzi, F., Vigato, P.A. (2011.) Electron Backscatter Diffraction (EBSD): A New Technique for the Identification of Pigments and Raw Materials in Historic Glasses and Ceramics. Archaeometry, 53(1), 178–193. https://doi.org/10.1111/j.1475-4754.2010.00540.x.

[21] Stojakovic, D. (2012). Electron backscatter diffraction in materials characterization. Processing and Application of Ceramics, 6(1), 1–13. https://doi.org/10.2298/PAC1201001S.

[22] Schwartz, A.J., Kumar, M., Adams, B.L., Field, D.P. (2009). Electron backscatter diffraction in materials science. 2nd edition, Springer, New York. ISBN: 978-0-387-88136-2.

[23] See http://www.ebsd.com/introduction for further details.

[24] Stebbins, J.F., Dubinsky, E.V., Kanehashi, K., Kelsey, K.E. (2008). Temperature effects on non-bridging oxygen and aluminum coordination number in calcium aluminosilicate glasses and melts. Geochimica et Cosmochimica Acta, 72, 910–925. https://doi.org/10.1016/j.gca.2007.11.018.

[25] Yurdakul, A., Günkaya, G., Kavas, T., Dölekçekiç, E., Karasu, B. (2014). Investigations on Fiber Production Attempts from the Borosilicate and SMFMZS (SrO-MgO-Fe_2O_3-Mn_2O_3-ZrO_2-SiO_2) Glass Systems. Afyon Kocatepe Üniversitesi Fen ve Mühendislik Bilimleri Dergisi, 14(OZ5701), 1-9.

[26] Fox, K.M., Edwards, T.B., Peeler, D.K. (2008). Control of Nepheline Crystallization in Nuclear Waste Glass. International Journal of Applied Ceramic Technology, 5(6**)**, 666–673. https://doi.org/10.1111/j.1744-7402.2008.02250.x.

[27] Deshkar, A., Gulbiten, O., Youngman, R.E., Mauroc, J.C., Goel, A. (2020). Why does B_2O_3 suppress nepheline ($NaAlSiO_4$) crystallization in sodium aluminosilicate glasses? Physical Chemistry Chemical Physics, https://doi.org/10.1039/D0CP00172D.

[28] Sitzman, S.D., Nolze, G., Nowell, M.M. (2010). EBSD Pattern Quality and its Use in Evaluating Sample Surface Condition. Microscopy and Microanalysis, 16, 698-699. https://doi.org/10.1017/S143192761005467X.

[29] Wright, S.I., Nowell, M.M. (2006). EBSD Image Quality Mapping. Microscopy and Microanalysis, 12, 72-84. https://doi.org/10.1017/S1431927606060090.